# In-Flight Verification and Validation of Colloid Microthruster Performance

John Ziemer[1], Colleen Marrese-Reading, Curt Cutler, Charles Dunn, Andrew Romero-Wolf, Shahram Javidnia, Thanh Le, Irena Li, and Phil Barela
*NASA Jet Propulsion Laboratory, California Institute of Technology, Pasadena, CA, 91109, USA*

Nathaniel Demmons[2] and Vlad Hruby
*Busek Company, Inc., Natick, MA, 01760, USA*

and
Jacob Slutsky[3], James Ira Thorpe, Peiman Maghami, Oscar Hsu, and James O'Donnell
*NASA Goddard Space Flight Center, Greenbelt, MD, 20771, USA*

**Colloid Micronewton Thrusters (CMNTs) use an electrospray to provide precision spacecraft position and pointing control. They were demonstrated in space for the first time as part of NASA's Space Technology 7 (ST7) payload hosted by the European Space Agency's (ESA's) LISA Pathfinder (LPF) technology demonstration mission in January, 2016. CMNTs were the actuator in the disturbance reduction system (DRS) that provided drag-free operation of the LPF spacecraft, which will be necessary for future gravity wave observatories such as ESA's Laser Interferometer Space Antenna (LISA) mission, currently in Phase A and scheduled for launch in 2034. The CMNT technology met performance requirements operating at 5-30 μN of thrust with 0.1 μN resolution and ≤0.1 μN/√Hz thrust noise to deliver the required nanometer-level precision spacecraft control measured by the gravitational reference sensor (GRS) in the ESA LISA Technology Package (LTP). The performance of seven of the eight CMNTs in flight was consistent with ground test results, and as a system, all eight thrusters met mission-level performance requirements. The colloid microthruster performance model of thrust and thrust noise as a function of operational parameters (i.e. beam current, voltage, temperature, etc.) was validated in flight over a wide range of conditions. A model and simulation of the thruster control algorithm was developed and validated with flight data to predict thrust noise. This capability is important for future missions because it relates directly to the acceleration noise on the test masses, which provide the gravity wave measurements. The CMNT thruster model data and validation with LISA Pathfinder/ST7-DRS flight experiments are presented in this paper.**

[1] LISA Microthruster Lead and ST7 Payload Systems Engineer, AIAA Member, john.k.ziemer@jpl.nasa.gov
[2] Micropropulsion Group Lead and Colloid Microthruster Cognizant Engineer, AIAA Member, nate@busek.com
[3] Microthruster Performance Analysis Lead, University of Maryland, jacob.p.slutsky@nasa.gov

## I. Nomenclature

$C_1$ = simple thrust coefficient
$C_2$ = more accurate thrust coefficient used with $V_{tc}$
$I_B$ = measured beam current
$T$ = calculated thrust
$V_B$ = measured beam voltage
$V_{BNOM}$ = nominal beam voltage set point (typically 6 kV)
$V_{tc}$ = loss due to energy in forming droplets at end of Taylor Cone emission jet

## II. Introduction

The primary objective of the Laser Interferometer Space Antenna (LISA) mission is to detect and measure gravitational waves produced by compact binary systems, mergers of super massive black holes, and other source of scientific interest. However, even interplanetary space is subject to minute disturbances, such as solar radiation photon pressure that could mask the influence of gravitational waves on free-floating test masses. LISA consists of a precisely controlled set of three spacecraft separated by 2.5 million kilometers that each provide two interferometric links between two free-floating test masses. The spacecraft must follow the test masses within approximately 10 nm and shield the gravitational wave instrument from any disturbances. Calculations have shown that to reach the sensitivity level of interest, the acceleration disturbances to the test masses may be no more than approximately $3\times10^{-15}$ m s$^{-2}$ Hz$^{-1/2}$ along the sensitive axis in the 1x10$^{-4}$ to 0.1 Hz bandwidth (the real sensitivity varies as a function of frequency and can be found in Ref. [1]). This extremely precise measurement requires microthrusters to control the spacecraft attitude and position with $\leq$0.1 $\mu$N/$\sqrt{}$Hz thrust noise to minimize disturbances in the bandwidth of interest. This introduction will provide an overview of the LISA Pathfinder technology demonstration mission and a summary of previous results.

### A. LISA Pathfinder

LISA Pathfinder (LPF) [2] was a European Space Agency (ESA) led technology demonstration mission that successfully demonstrated the performance of key technologies for LISA from January 2016 to July 2017 [3,4]. LISA is ESA's next large mission (L3) concept, which is currently in Phase A of development and expected to launch in 2034 [1,5]. Space Technology 7 - Disturbance Reduction System (ST7-DRS) [6] was a NASA payload on LPF managed by the Jet Propulsion Laboratory (JPL) including partnerships with Busek Company, Inc. to provide Colloid Micro-Newton Thrusters (CMNTs) [7-9] and Goddard Space Flight Center (GSFC) to provide the Dynamic Control System (DCS) software [10-12].

The goal for LISA Pathfinder and ST7 was to demonstrate key DRS technologies in just one spacecraft, consisting of two free floating test masses with capacitive position sensors in the Gravitational Reference Sensor (GRS), microthrusters as precision position control actuators for the spacecraft, and drag-free control laws that maintain the spacecraft position and cancel out the environmental disturbances, mainly due to solar photon pressure, that can loosely couple to the test masses providing noise on the gravitational wave strain measurement. An exploded view of the LISA Pathfinder spacecraft is shown in Figure 1. ESA developed the LISA Technology Package (LTP) for LPF that included a GRS and a laser interferometer for precisely measuring the relative position of the test masses along one axis and "tip-tilt" angles perpendicular to the sensitive axis. While LPF used six cold gas microthrusters and their own Drag-Free Attitude

Control System (DFACS), the ST7 payload used eight colloid microthrusters and the DCS with the sensing provided by the LTP.

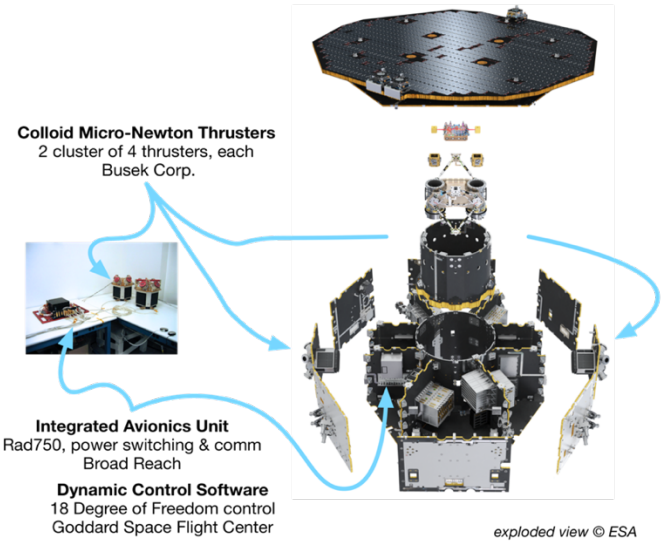


**Figure 1. Exploded view of the LISA Pathfinder spacecraft with the ST7 DRS payload.**

LISA Pathfinder launched in December of 2015, performed commissioning activities including the first successful activation of the ST7 payload colloid microthrusters [13] in early January of 2016, and reached its final Earth-Sun L1 orbit on January 22, 2016. During the transfer-phase commissioning activity, the propulsion module was still attached to the spacecraft, and the test masses were held safely in place by static launch locks. All 8 CMNTs started and cleared bubbles in the expected 3-day timeframe; however, Thruster 1 showed signs of reduced response time and additional thrust noise caused by a single emitter rapidly turning on and off (this anomaly will be discussed more later in the paper). During this phase of the mission, thrust was measured to within 10% by on-board gyroscopes and showed the DRS meeting all thrust range performance requirements, which allowed the CMNTs to be considered as a potential backup to the cold gas microthrusters for de-spin and tip-off corrections after the propulsion module separated. After separation from the propulsion module, the cold gas thrusters completed the de-spin and tip-off corrections without needing the colloid thrusters, and the colloid thrusters were safely shut down. LTP instrument commission continued successfully, including test mass releases, and the ESA-led experiment commenced on March 1, 2016.

After the successful set of ESA experiments [3], ST7-DRS began its instrument phase commissioning on June 26, 2016 and its nominal mission on August 14, 2016. This period of operations was focused on restarting the colloid thrusters, demonstrating control of the spacecraft attitude, and developing a work-around for a thruster computer memory anomaly. During phases of the LPF mission where ST7-DRS operated, NASA's colloid thrusters were used in place of ESA's cold gas thrusters to move and orient the spacecraft, with the DRS control laws replacing the ESA control laws. An illustration of the DRS concept is in Figure 2. During ST7 operations, the rest of the LTP payload played the same role as during the LTP-led parts of the mission, by providing information on the positions and attitudes of the test masses and applying forces and torques to the test masses, as requested by the DRS controllers. The primary purpose of the ST7-DRS operations was to measure and characterize the performance of the microthruster and DCS subsystems, with consideration for their potential use in LISA or other missions. Experiments

were conducted with the ST7-DRS to control the spacecraft through different drag-free control modes, observing test mass position and acceleration noise, calibrating the thrusters and validating the performance model and control algorithm model simulations. Eleven significant experiments were conducted during the primary mission and fourteen were conducted during the extended mission. The DRS met all of its mission-level requirements, successfully demonstrating the required performance of the CMNTs and the DCS control laws [14-16].

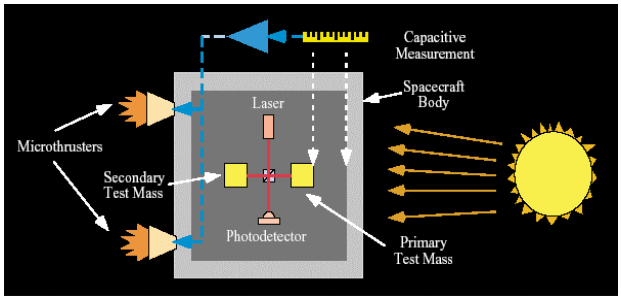


**Figure 2. An illustration of the DRS concept. [6]**

**B. Colloid Micronewton Thrusters (CMNTs)**

The two Colloid Micronewton Thruster Assemblies (CMTAs) are identical units provided by Busek Co., Inc. [7-9]. A single unit with four thrusters is shown in Figure 3 with a functional block diagram. A thruster assembly includes: 4 thruster heads, 4 propellant feed systems, 4 Power Processing Units (PPUs), 1 cathode, and 1 Digital Control Interface Unit (DCIU). The thruster heads and feed systems are independently controlled through the PPUs, which are controlled, in turn by the DCIU. The DCIU has a power, command, and telemetry interface to the DRS integrated avionics unit (IAU) that houses the DRS command and data handling flight software, including the DCS. The DCIU also controls the cathode neutralizer. The DCIU has an on-board PROM (programmable read-only memory) that stores the thruster operating software and control algorithms. The CMTA mass is 14.8 kg. The nominal power for the CMTA 1 and 2 are 16.5-17.1 W with all four thrusters running, with a maximum power of 24.6 and 25.4, respectively, when heaters are operated at full power. Each thruster head includes a manifold that feeds nine emitters in parallel, a heater to control propellant temperature and physical properties, and electrodes that extract and accelerate propellant as charged droplets. The propellant is an ionic liquid 1-ethyl-3methylimidazolium bis(triflouromethylsulfonyl)imide (EMI-Im).

The thruster electrical schematic is shown in Figure 4. The thrust from each head can be throttled from 5 to 30 μN by changing the beam voltage (2000-8000 V) and/or the propellant flow rate that determines the beam current (2.25-5.4 μA). Independent, fine control of both the beam voltage and beam current allow for precise control of thruster to better than 0.1 μN resolution with <0.1 μN/√Hz thrust noise. The nominal specific impulse is 240 s. Propellant is stored in four electrically isolated steel bellows compressed by four constant force springs set to supply four microvalves with propellant at approximately 1 atm of pressure. The microvalve is piezo-actuated (developed at Busek) using ~1 mW of power to control the propellant flow rate and current to better than 1 nA with a response time over its full range of less than 0.5 s. Limits on analog to digital converters and telemetry bandwidth brought the resolution down to 6 nA, corresponding to about 0.1 μN of thrust on orbit. The thruster performance requirements and performance during ground tests and operations in flight are summarized in Table 1.

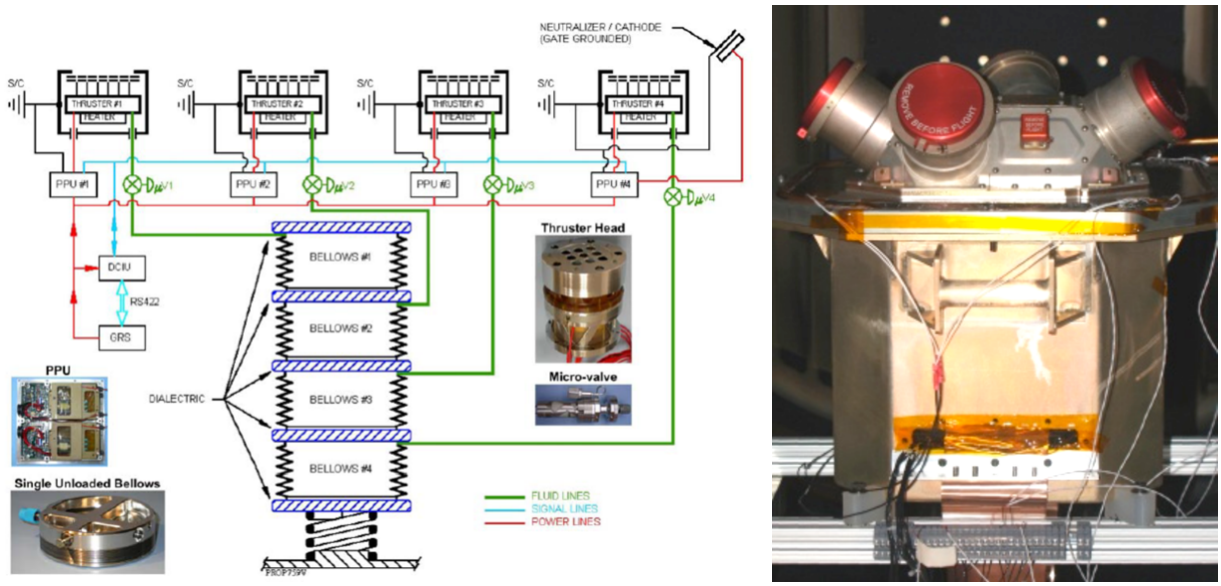


**Figure 3. CMNT cluster functional block diagram with pictures of various components (left) and the Busek Colloid Micro-Newton Thruster (CMNT) Flight Cluster 1 including four thruster heads, electronics, and cathode neutralizer (visible) in thermal-vacuum environmental test setup (right) prior to delivery [7-9].**

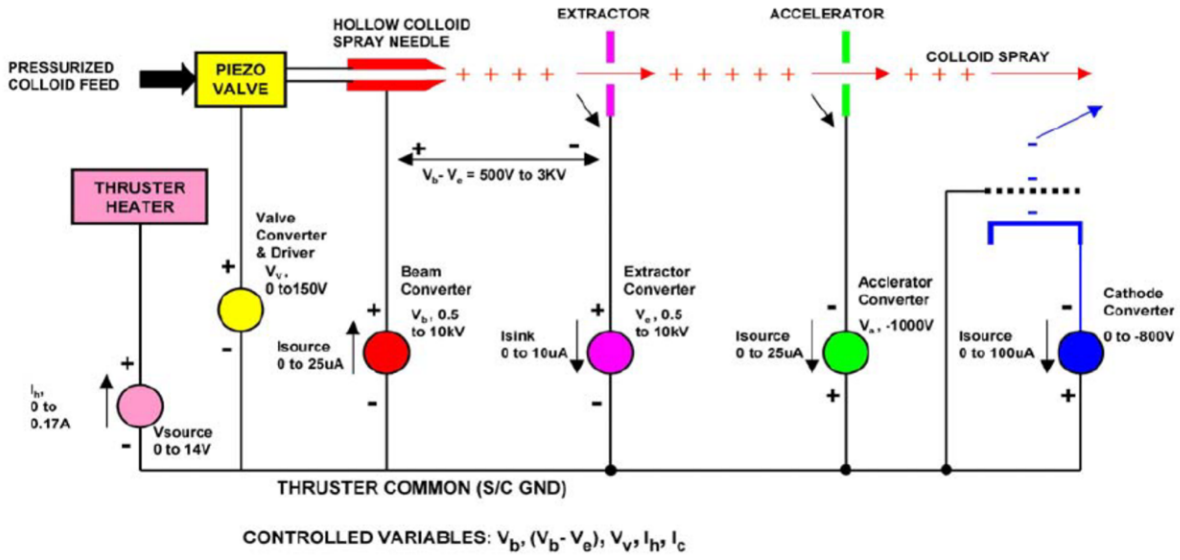


**Figure 4. Thruster electrical schematic showing beam, emitter, extractor, accelerator, and cathode neutralizer voltage sources [7-9].**

The cathode neutralizer developed by Busek is made from carbon nano-tube (CNT) base with an extractor electrode. The cathode is capable of producing 10 µA to 1 mA using extraction voltages of 250 to 800 V. One CNT cathode was tested over 13,000 hours at 100 µA without incident and CNT cathodes were tested successfully with operating thruster heads in each full functional test during the thermal environment qualification tests for each unit prior to launch. During these tests, Cluster 1 cathode demonstrated 13 µA at 242 V and 23 µA at 268 V and Cluster 2 cathode demonstrated 13 µA at 375 V and 26 µA at 420 V.

**Table 1. CMNT performance requirements and performance summary on the ground using an engineering model (EM) and in flight on all 8 flight units.**

| Performance Parameters | ST7 Requirement | Ground Tests (EM) | Demonstrated in Flight | | | | | | | |
|---|---|---|---|---|---|---|---|---|---|---|
| | | | Thr 1 | Thr 2 | Thr 3 | Thr 4 | Thr 5 | Thr 6 | Thr 7 | Thr 8 |
| **Thrust Range (μN)** | 5 to 30 | 4.35 to 35.8 | 5-30 | **5-50** | 5-30 | 5-30 | **5-60** | 5-30 | 5-30 | 5-30 |
| **Thrust Precision (μN)** | ≤0.1 | 0.08 (0.01 calculated) | ≤1 | ≤0.1 | ≤0.1 | ≤0.1 | ≤0.1 | ≤0.1 | ≤0.1 | ≤0.1 |
| **Thrust noise (μN/√Hz)** | ≤0.1 | ≤0.01 ($3x10^{-5}$ to 3 Hz) <0.1 (3-4 Hz) | ≤0.8 | ≤0.1 | ≤0.1 | ≤0.1 | ≤0.1 | ≤0.1 | ≤0.1 | ≤0.1 |
| **Thrust Range Response Time (s)** | ≤ 100 s | < 10 s | 147 s | <10 s | <10 s | <10 s | <10 s | <10 s | <10 s | <10 s |
| **Operational Lifetime (hours)** | any measurable thrust on-orbit* | 3478 hours during FLT 2B (245 Ns of impulse) | >2400 hrs (100 days) | >2400 hrs (100 days) | >2400 hrs (100 days) | 1690 hrs, (70 days) | >2400 hrs (100 days) | >2400 hrs (100 days) | >2400 hrs (100 days) | >2400 hrs (100 days) |
| **Propellant mass sprayed (grams)** | none | 113 | 74.8 | 67.02 | 84.1 | 68.89 | 64.46 | 59.05 | 91.07 | 89.52 |

* Given the unplanned 7+ years they sat, fully fueled after delivery. The mission lifetime requirement was 60 days for the nominal mission with a design goal of ≥2160 hours (90 days) to support an extended mission as well.

The thruster electronics includes 4 power processing units (PPUs) and one digital control and interface unit (DCIU) for each cluster. The PPU includes the high-voltage DC-DC converters that have been specifically designed and tested for this application by Busek Co. and proved to be very robust without any failure in ground or on-orbit testing. The DCIU controls all four thrusters and provides the command and telemetry interface to the spacecraft and DRS flight computer. The thruster control algorithm with the thruster performance model run in the DCIU to receive thrust commands and voltage and current telemetry to determine and send the next voltage commands to the PPU. The DCIU can also operate in a pass-through mode with voltage commands determined by the control algorithm running in the flight software in the IAU instead, as was demonstrated during the LISA Pathfinder Mission.

### C. Dynamic Control System (DCS)

The flight software implementing the DRS Dynamic Control Software (DCS) algorithm resides in the IAU and was used to control the spacecraft and the test masses. It performed this function by computing thruster force commands to maintain spacecraft attitude and test mass force and torque commands for drag-free operation based on spacecraft attitude and test mass positions and attitudes received from the LPF On-Board Computer (OBC). Its functions included sensor processing (from LTP and LPF), control filters propagation, actuation command generation (thrust commands and electrostatic actuation commands) and internal fault notification. The on-board data handling (OBDH) of the OBC interacts with the DRS C&DH software on the IAU to pass commands and telemetry back and forth. The OBC stores ground commands on the mission timeline (MTL) and telemetry from the DRS.

There are several DRS and DCS modes with different internal subsystem states within each mode. The DRS instrument enters a certain mode when the subsystems take on unique states within each mode. Each subsystem state may be commanded independently with the configuration options presented in . **Initialization/Safe Mode (Init or Safe)** is the mode the DRS instrument enters upon power being applied from the spacecraft. Only the IAU had power in this mode. This was also the instrument's Safe mode. **Standby Mode** was the mode in which

the DRS was not controlling either the spacecraft or the LTP test masses, and its IAU and thrusters were on but disabled. Standby Mode was considered the initial mode for DRS operations. When the DRS thrusters are on and being commanded, they are commanded in one of two ways. In **Thruster Command Mode (ThrCmd)**, the thrust level of each thruster is directly commanded and the DCIU determines the operating current and voltage levels to comply with the command. **Thruster Diagnostic Mode (ThrDiag),** as initially implemented, is a mode in which the DRS is not controlling either the spacecraft or the LTP test masses, its IAU and thrusters are on and enabled (thruster DCIU is on, PPUs are enabled) into diagnostic mode. This allows the thrusters to operate based on current and voltage commands (each thruster can be commanded independently) from the IAU. This mode was only expected to be used during commissioning phases or thruster fault diagnosis and recovery activities, but after a PROM anomaly in the DCIU, the mode implementation was adjusted to allow its use while the DRS was controlling the spacecraft, and then the mode was used for most of the rest of the mission.

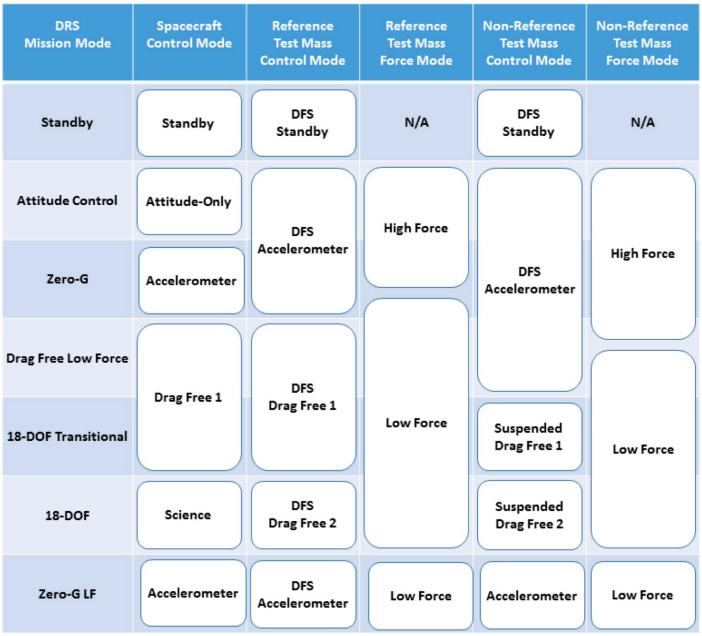


**Figure 5. Table of all DCS modes include state of the spacecraft, test masses, and DCS controllers. Take from [16].**

When DRS is in control of the spacecraft, the DCS uses five control modes. **Attitude Only Control Mode (ATT)** stabilized the attitude of the spacecraft and the attitude and position of test masses after handover from the LPF without compensating for solar pressure. Both test masses had their position and attitude controlled in a "high force" (wide range) mode and the DCS test mass controllers were both in accelerometer mode. Spacecraft attitude was controlled by the micro-newton thrusters. **Zero-G Mode (ZG)** maintained spacecraft and test mass states while opposing solar pressure and other secular forces acting on the spacecraft using the micro-newton thrusters. Both test masses were either in high force (wide range) or low force (high precision) mode and the DCS test mass controllers were both in accelerometer mode to operate the test masses as accelerometers. Spacecraft attitude was also controlled by the micro-newton thrusters. This mode was used to measure thruster thrust levels by measuring the test mass motions and forces required to keep them in a fixed position and non-rotating in their housing. This was the main mode used for independent thrust measurement. **Drag-Free Low Force (DFLF)**

established drag-free motion about the reference test mass using the micro-newton thrusters. The reference test mass transitioned into Low-Force (high resolution) mode, with no electrostatic force commanding to control position (the spacecraft position was controlled around the reference test mass by the microthrusters and DCS), although small torque commands were used. This mode was designed to be the quietest mode in terms of amplitude of thrust command variations and expected thruster noise while operating one test mass in drag-free mode. A transitional mode, **18 Degree-of-Freedom Transitional (18-DOF-Trans) Mode and Science Mode (18-DOF)** was the second drag-free mode and the highest control mode for the DRS, controlling all 18 degrees of freedom with the highest fidelity. This was the expected mode for LISA science operations with the both test masses freely floating and the spacecraft attitude stably controlled by the colloid thrusters. In this mode, drag free motion was to be maintained for two test masses along the sensitive axis and within the DRS bandwidth.

The DCS provided both attitude and drag free control with the required performance with the colloid thrusters. It was required to maintain the spacecraft Z axis to an absolute accuracy of 2 degrees (3 sigma) half cone angle with respect to the Sun vector and the rotation around the Z axis to an accuracy of 2 degrees (3 sigma) with respect to the steering law. It was required to maintain the spacecraft position with respect to the test masses, about the sensitive axis (x-axis of the LTP housing frames H1 or H2), to better than 10 nm/√Hz in the measurement bandwidth (MBW). The measurement bandwidth covers the frequency range of 1 mHz to 30 mHz. The performance of the DRS in meeting all off the mission requirements is presented elsewhere [14-16] with this paper focusing on the performance of the CMNT thrusters.

## III. Thruster Performance and Control Algorithm Models

The DRS used a simplified version of the thruster performance model in the thruster control algorithm with 8 thrusters in a closed loop control with the DCS to control spacecraft attitude and spacecraft position and angles relative to the free-falling test masses. This section describes the thruster performance model, control algorithm and the simulation of it.

### A. CMNT Thrust Performance Model

The thrusters were controlled using the performance model in the thruster control algorithm. The functional form of the colloid thruster thrust model is given in Equation 1. It provides the relationship between thrust level, T (micronewtons), the beam current, $I_B$ (microamperes), applied beam voltage, $V_B$ (volts), and thrust coefficient, $C_1$, which is mainly dependent on the charge-to-mass ration of the droplets and a function of the propellant physical properties (i.e. conductivity, surface tension, etc.) and various loss mechanisms (i.e. beam spreading, non-uniform charge-to-mass ratio, propellant utilization, etc.) including the energy lost in forming the charged droplets of the electrospray. $C_1$ was determined on the ground prior to launch and found to be a strong function of temperature and the water content of the propellant. Later tests showed that a more accurate thrust performance model includes the droplet energy loss term separately, $V_{tc}$, with a new thrust coefficient, $C_2$ (Equation 2). The differences between the two relationships matter most at lower beam voltages where $V_{tc}$ has more of an influence.

$$T = C_1 I_B^{\frac{3}{2}} V_B^{\frac{1}{2}} \quad (1)$$

$$T = C_2 I_B^{\frac{3}{2}} (V_B - V_{tc})^{\frac{1}{2}} \quad (2)$$

ST7-DRS used the simplified version of the performance model (Eq. 1) for thruster control that was validated on a thrust stand. The thrust, and the beam current and voltage were measured with an Engineering Model (EM) thruster horizontally supported on a magnetically levitated thrust stand with micronewton resolution. Thrust was measured in the 5-30 μN range to estimate the thrust coefficient, $C_1$. The thruster was operated at room temperature, close to 25°C, and the propellant was dry to ≤150 ppm water content. The efficiency and $V_{tc}$ terms were not fully characterized for the ST7 CMNTs prior to when the model needed to be finalized for the thruster and DCS controller designs and software delivery. With this simplified version of the performance model at constant thrust levels, the delivered thrust performed within 2% of the commanded thrust at nominal voltages, currents and temperature and with a $C_1$ of 0.0319. The nominal temperature was 25°C. The nominal beam voltage was 6000 V with a range of 4000-8000 V. The nominal extraction voltage was 1600 V. The current range was 2.25 – 5.3 μA. At non-nominal voltages, Taylor cone losses and beam divergence effects can impact the thrust by >2% for beam voltages at 4000-8000 V. Taylor cone losses impact the thrust by ≤ 8 % for the full range of typically allowable beam voltages (2000-10000 V). Temperature also influences the value $C_1$, which decreases with increasing temperature. The values of $C_1$ at different temperatures have been predicted using models including the physical properties of the propellant and verified by measurement. This performance model was validated using a single thruster EM unit on a thrust stand, and the model was then used to verify that the 4 CMTA flight units in each cluster met requirements because they were too heavy for direct measurements on the thrust stand. The $C_1$ values estimated from ground measurements are 0.0372 at 15°C, 0.0343 at 20°C, 0.0298 at 30°C with the largest uncertainty being in the actual temperature of the emitters during the ground testing. These values of $C_1$ were used in the thruster control algorithm for the flight experiments at these temperatures.

**B. CMNT Control Algorithm and Model Simulation**

To take thrust commands from the DCS or DFACS and translate them to current and voltage setpoints, a CMNT control algorithm is used either on board the DCIU or with the flight software on the IAU. The thruster control algorithm was developed by Busek and implemented on the DCIU by Vtech Engineering Corporation [8]. The control algorithm was programmed into the PROM in the DCIU and could not be changed once the software was burned into the PROM during cluster assembly and approximately 1 year prior to delivery. A back-up copy of it was also programmed into the DRS C&DH flight software in the IAU, which could be updated and was used instead for most of the mission after the Cluster 2 DCIU memory anomaly. The DRS Drag-Free Control Software resides in the IAU and is responsible for computing thruster force commands to maintain spacecraft attitude and test mass force and torque commands at 10 Hz for drag free operation based on the spacecraft attitude and test mass position and attitudes received from the On-Board Computer (OBC). The OBC resides on the LISA Pathfinder (LPF) spacecraft and acquires this telemetry from the LISA Technology Package (LTP).

The thruster control model translates high level thrust commands from the IAU into the low-level voltages required by the local Power Processing Units (PPU) to control the thrusters including beam voltage, extraction voltage (the difference between beam and extractor electrode converters), and microvalve voltage. It takes the measured current and voltages to calculate thrust level using the simplified performance model, compares it to the new thrust command and then calculates the new beam current, then beam voltage and then the propellant flow control voltage to command for each thruster. It limits the voltage and current ranges and the changes in them in each cycle. A flow diagram for the model is given in Figure 6 [8]. It executes every real

time interval (RTI) of 100 ms, and completes within 70 ms for all 8 thrusters, sending a telemetry packet of the current and voltage read out at the beginning of the cycle. The objective of the algorithm is to drive the thrust error to zero as soon as possible by controlling the beam voltage and current. The thrust error is the difference between the thrust calculated using performance equation and measured beam current and voltage and the thrust command from the IAU. The algorithm also has a requirement to have the beam voltage converge to a nominal beam voltage, $V_{BNOM}$, to ensure that the thrusters are operating at an average voltage that allows both bidirectional headroom for the beam voltage adjustments and ensures that over the long term, the average specific impulse is at a desirable value.

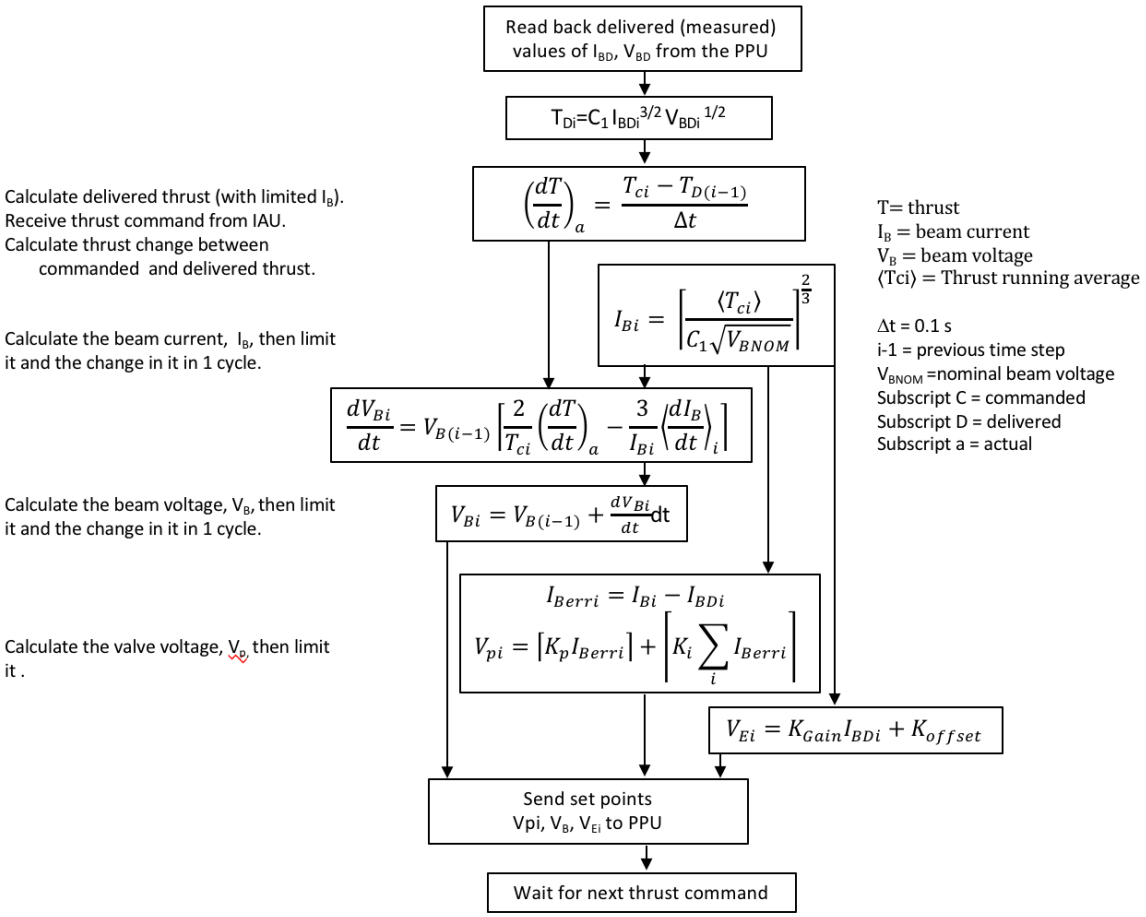


**Figure 6. Primary elements of the CMNT thrust control algorithm [8].**

A model simulation was developed of the thruster control algorithm in the commercial Wavemetrics Igor data analysis tool to predict thruster performance and noise assuming a simple fixed gain for the beam current derived from the microvalve voltage command. It can be used to test potential improvements in various parameters in the control algorithm to improve the performance of the colloid thrusters and the DRS in flight to reduce the thrust noise on the spacecraft. This model follows the algorithm flow diagram and details shown in Figure 6. It uses the same data types and limited precision for the various controlled and monitored parameters as programmed into the DCIU and the DRS C&DH flight software. It includes nominal beam voltages and maximum and minimum voltage and current values. It includes

maximum current and voltage step sizes per cycle (0.1 s). It includes proportional and integral gains on the piezo valve controller to control the mass flow rate of the propellant and the beam current. It also includes a 3-cycle timing delay in the telemetry that resulted from the control algorithm running in the FSW in the IAU instead of the DCIU, once that change was made early in the mission and prior to all experiments.

## IV. Model Validation Approach

The performance and thruster control models were verified in flight with the DCS control models by meeting the mission control and performance requirements and then verified per thruster for all 8 thrusters by measuring the thrust from each thruster and using models of the DRS to estimate the thrust coefficients. A model simulation of the thruster control algorithm was developed to predict delivered thrust profiles for thrust command profiles to estimate thruster noise and study the impact of thruster anomalies and control algorithm changes on thruster noise. It was also validated against flight data and applied to show how the CMNT propulsion system noise performance was better than the 1 Hz telemetry data suggested and how it could be improved for future missions. This section of the paper discusses the approaches developed to validating the models with flight data.

### A. Performance Model Validation Approach

The thruster performance model was validated before flight by measuring the thrust, beam current and beam voltage and verifying that they agreed within the required accuracy over the mission thrust range of 5-30 μN. Thrust measurements were taken on the ground with engineering model thrusters using a magnetically levitated thrust stand. The nominal thrust stand accuracy was 2% and the temperature control was accurate to within 2 degrees Celsius. As discussed in the previous section, at non-nominal voltages, Taylor cone losses and beam divergence effects impacted the thrust by <2% from the model prediction with a constant $C_1$ and $V_{tc}$ set equal to zero for beam voltages between 4-8 kV and ≤10% for the full range of typically allowable beam voltages (2-10 kV). Because of the closed loop spacecraft control approach with 8 thrusters, delivering the required thrust to within 10% accuracy was acceptable with 0.1 μN thrust control precision.

The thruster performance model was validated in flight by the DRS. The LISA Technology Package (LTP) inertial sensor was used to measure the delivered thrust level of each of the thrusters and verify the thrust model in flight. Because the test masses were not physically connected to the spacecraft, the LTP measured positions and actuation of the test masses could be used to estimate the forces and torques applied to the spacecraft [14-16]. This measured thrust was compared to the beam current and voltage and the performance model to estimate $C_1$. Experiments were conducted for nominal current, voltage, and temperature, as well as for off-nominal values. Because the thrusters were simultaneously being used to control the spacecraft attitude, arbitrary injections were not possible in flight. Therefore, the bulk of experiments involved adding sinusoidal injections at several chosen frequencies above the bandwidth of the attitude controller and smaller amplitudes (~1 μN), to allow good signal to noise while preserving system stability. In one experiment, the test masses were injected with position signals, which helped with calibration of the applied forces and torques vs. commanded values. The modeled thruster response compared to the measured response can be used to estimate the average $C_1$ for all of the thrusters.

### B. Control Algorithm Model Simulation Validation Approach

The approach to validating the control model was to demonstrate that it could deliver the required thrust command profile expected and meet the thruster noise requirements and spacecraft attitude and position requirements. Acceptance tests were conducted before flight with expected thrust command profiles. These tests were done with thrust command profiles for the highest control mode expected in flight, which was the 18DoF mode. All 8 thrusters demonstrated approximately the required thruster noise level (difference between thrust calculated with the model and commanded thrust) for DC thrust commands of 0.1 μN/√Hz during the ground tests with AC thrust commands. The control model was validated in flight in all of the DRS modes including 18DoF. In flight, the control model was validated by maintaining the required spacecraft attitude and position control in all of the DRS modes while meeting the thruster noise requirement of 0.1 μN/ Hz in the 1-30 mHz frequency range.

The approach to validating the thruster control algorithm model simulation was to compare the thrust noise calculated from the thrust profiles predicted by the model with the thrust noise calculated from the flight thruster thrust profiles. The thrust noise was estimated by taking the Power Spectral Density (PSD) of the difference between the calculated and commanded thrust. The thrust is calculated from the current and voltage telemetry using the performance model. Thrust noise profiles were compared for different DRS modes in the validation process. Experiments were conducted to change various control algorithm parameters to show that the simulation could predict the results observed in flight. The simulation included a telemetry delay of 3 cycles (0.3 s) in the thruster parameters including beam current and voltage that resulted in voltage oscillations. This delay was a result of running the thruster control algorithm in the IAU instead of the DCIU after it was required because of a DCIU anomaly. The validated simulation was used to show the expected improvement in noise spectra without this and another flight anomaly. It can also be used to explore approaches to reducing thruster noise by improving the control algorithm.

## V. Results and Discussion

### A. Performance Model Validation Results

The thruster performance model, control algorithm and DCS control laws were verified by the DRS using them to maintain the required attitude and spacecraft position control in each of the DCS modes. Figure 7 shows several minutes of thrust command telemetry and calculated thrust as calculated from the thruster beam voltage and current telemetry using the thruster performance model. The spacecraft attitude errors and test mass position and angles are in Figure 8 showing that the DRS met the S/C attitude error requirement at ≤2 deg. (35 millirad). The test mass position requirement was 10 nm/√Hz at 1-30 mHz. The bump in the data is suspected to be a micrometeoroid impact and is included in these figures to show a higher transient command case. Figure 7 shows that the thrusters and DCS responded to the disturbance and the thruster thrust level (markers) followed the thrust commands (solid lines) very well. Figure 8 shows that the DRS maintained the spacecraft position and attitude requirements, even during a significant disturbance in 18DoF. The spacecraft position was temporarily displaced by about 150 nm from the impact. Earlier papers [17-20] show additional results from the first phases of the ST7-DRS mission (including cold gas thrusters and ESA's use of the colloid thrusters in their own operations) while the rest of this paper focuses on validation of the thrust and thrust noise performance model and control algorithms.

The LISA Technology Package (LTP) inertial sensor was used to measure the delivered thrust level of each of the thrusters and verify the thrust model in flight. It was used to measure the position and attitude of the test masses for calculations of the forces and torques applied to the spacecraft. Figure 9 presents both the thrust level predicted along the 3 axes (T6_CMNT_x.y.z) as calculated from the current and voltage measurements using the thruster model, and the thrust level calculated using the averaged data from both of the gravitational reference sensors (T6_GRS_x,y,z) in flight, for comparison. The agreement demonstrated was sufficient for the DRS to achieve the required noise performance for LISA Pathfinder. These thruster functional test data were collected during commissioning with ESA cold gas thrusters in operation that contributed to the noise in the measurements. The x-axis measurements were acquired with greater sensitivity and less noise using the optical interferometer, as shown in Figure 9. The measurements on the y and z axes were made with the electrostatic metrology system.

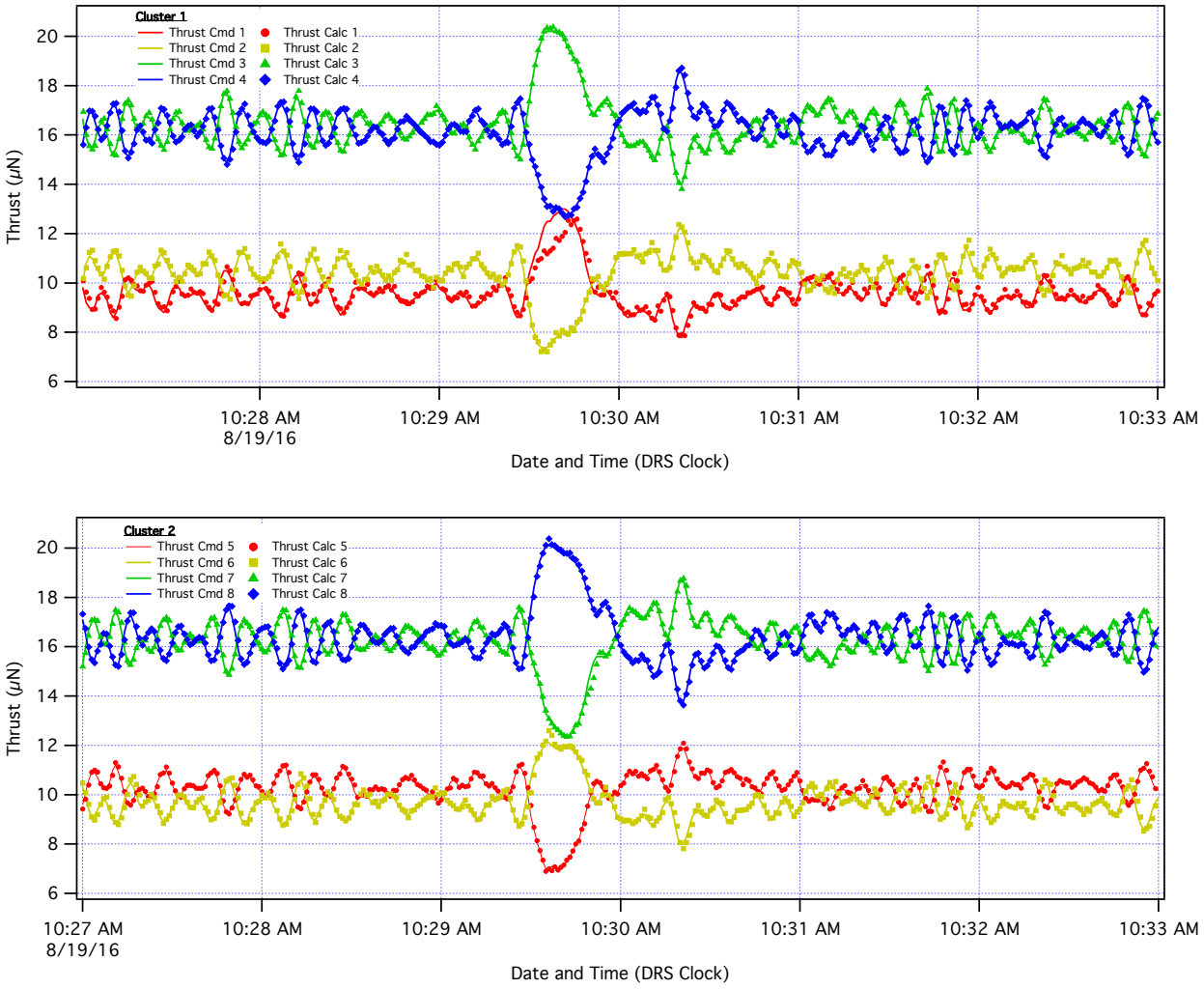


**Figure 7. Thruster command (Solid line) and calculated (markers) thrust levels that were achieved, validating the performance model and control algorithm in the flight demonstration of spacecraft attitude and drag-free test mass position control in 18-DOF with a suspected micrometeoroid impact to the spacecraft on DoY 232 (August 19, 2016).**

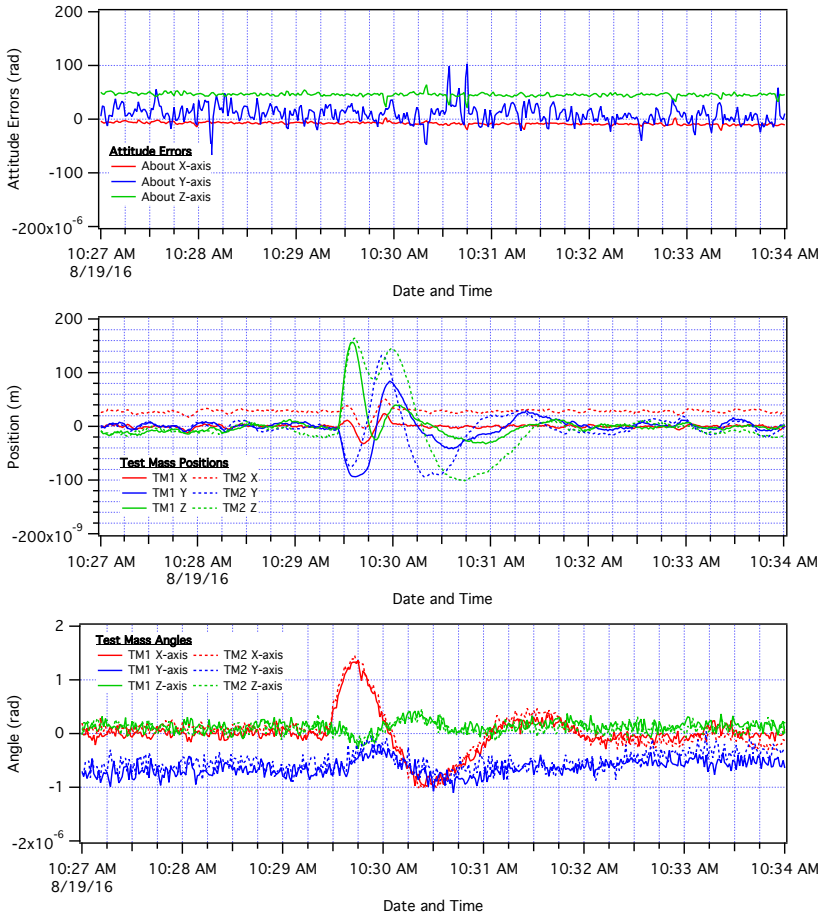


**Figure 8. Spacecraft attitude error, and test mass position and angles validating the performance model and control algorithm in the flight demonstration of spacecraft attitude and drag-free test mass position control in 18DoF with a suspected micrometeoroid impact to the spacecraft DoY 232 (August 19, 2016).**

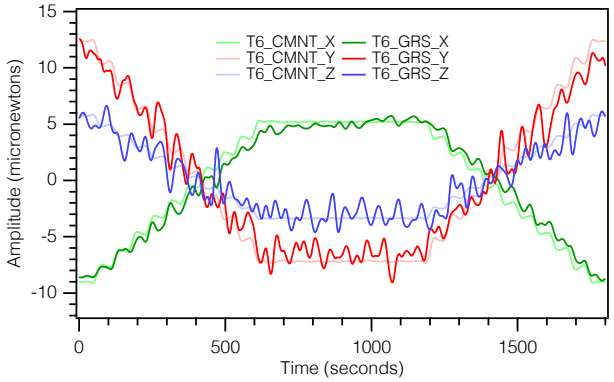


**Figure 9. Thruster 6 thrust on x, y, z axis calculated using thrust model and current and voltage measurements and using the spacecraft gravitational reference sensor (GRS) to measure thrust. Data shows good agreement between calculated and measured thrust.**

Multiple experiments were conducted to measure thrust using the LTP sensor to further validate the thruster performance model by measuring thrust and verifying the $C_1$ value. While the DCS was in a Zero-G mode, one thruster at a time was injected with 3 or 5 μN amplitude signals, with 23, 29, and 40 mHz sinusoidal thrust signals on top of the DCS thrust levels commanded. Using the thruster performance model with the measured thrust and beam current and voltage, the thruster constant $C_1$ was estimated for the measured thrust. These injections were also done at different temperatures for all 8 thrusters to investigate how $C_1$ changed with temperature in comparison to estimated values from models and ground measurements before flight. The results are presented in Table 2. The table includes the $C_1$ values estimated from the thrust stand (T/S) measurements and from the thrust measurements on the spacecraft. During the primary mission these experiments were conducted in a high force accelerometer (Zero-G) mode. A low force accelerometer mode was added before the primary mission because it improved the position measurement precision. It further improved the measurement precision to only measure position along the x-axis because of the interferometer measuring position along that axis. The thruster signal injections were then repeated for all of the thrusters. The results of this experiment are in Table 3. The results from this experiment conducted multiple times during the primary and extended mission are included in the graphs in Figure 10.

The results show that the $C_1$ estimates from thrust measurements in flight are lower than the estimates from thrust measurements on the thrust stand by as much as 10%. $C_1$ estimates are very similar for all of the thrusters but vary by <5% percent from their average value estimated, possibly indicating the level of error in the calibration of the high-force mode of the GRS, in the on-orbit measurement, or a slight variance from thruster-to-thruster. Relative changes in $C_1$ with temperature agreed within 1.5% of pre-flight estimates and those used in the flight experiments. In addition, measurements shown in Table 3 using the higher resolution Zero-G mode of the GRS show a better agreement with the ground-based measurements, again indicating a potential calibration error in the actual forces and torques applied to the test masses to compensate for the thruster signal injections. A graph of the $C_1$ estimates from the flight experiments is included in Figure 10. Months of operations were conducted successfully with a $C_1$ value of 0.0287 and several months were conducted with a value of 0.0319. These results suggest that the different thruster $C_1$ values were acceptable in the closed loop control DRS and that the largest discrepancy between the two values may have been from actual ground and on-orbit operating temperature at the emitter tip.

**Table 2. $C_1$ values estimated for each of the thrusters from the thrust, beam current and beam voltage measurements on the spacecraft in "high force" (low resolution) mode and from ground tests on a thrust stand (T/S row) at different temperatures.**

| Thr | C1x1000 15°C | +/- | C1x1000 20°C | +/- | C1x1000 25°C | +/- | C1x1000 30°C | +/- |
|---|---|---|---|---|---|---|---|---|
| **T/S** | **37.2** | | **34.3** | | **31.9** | | **29.8** | |
| **1** | 36.7 | 0.1 | 35.2 | 0.09 | 30.8 | 0.08 | 29.2 | 0.08 |
| **2** | 35.2 | 0.07 | 31.8 | 0.07 | 29.9 | 0.06 | 27.9 | 0.06 |
| **3** | 35.0 | 0.07 | 30.9 | 0.06 | 30.0 | 0.06 | 28.1 | 0.06 |
| **4** | 37.4 | 0.08 | 33.8 | 0.07 | | | | |
| **5** | 35.4 | 0.07 | 32.1 | 0.07 | 30.7 | 0.06 | 28.0 | 0.06 |
| **6** | 35.5 | 0.08 | 32.5 | 0.07 | 29.7 | 0.06 | 27.7 | 0.06 |
| **7** | 37.1 | 0.08 | 33.4 | 0.07 | 31.3 | 0.06 | 28.5 | 0.06 |
| **8** | 37.1 | 0.08 | 33.8 | 0.07 | 30.6 | 0.06 | 27.9 | 0.06 |
| **AVG** | **36.2** | | **33.0** | | **30.5** | | **28.2** | |

**Table 3. C1 values estimated for each of the thrusters from the thrust, beam current and beam voltage measurements on the spacecraft in "low force" (high resolution) mode and from ground tests on a thrust stand (T/S row) at 25°C.**

| Thr | C1x1000 | +/- | Delay | +/- |
|---|---|---|---|---|
| T/S | 31.9 | | | |
| 1 | 31.9 | 0.1 | -0.48 | 0.02 |
| 2 | 30.9 | 0.1 | -0.25 | 0.02 |
| 3 | 32.1 | 0.1 | -0.12 | 0.01 |
| 4 | | | | |
| 5 | 31.5 | 0.1 | -0.13 | 0.02 |
| 6 | 30.9 | 0.1 | 0.02 | 0.02 |
| 7 | 30.4 | 0.1 | -0.33 | 0.02 |
| 8 | 30.5 | 0.1 | -0.48 | 0.02 |
| Avg | 31.2 | | | |

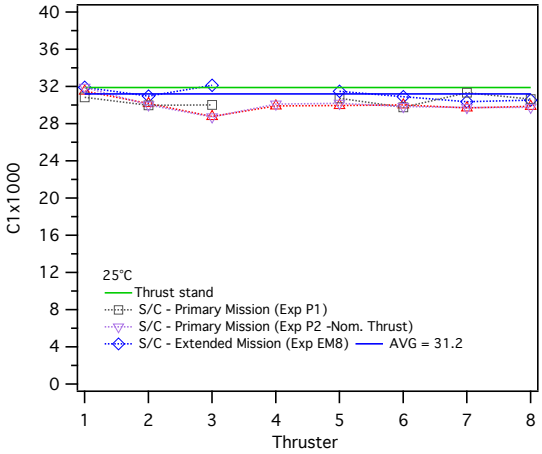


**Figure 10. C1 values estimated from thrust measurements on the spacecraft the same temperature during experiments throughout the primary and extended mission.**

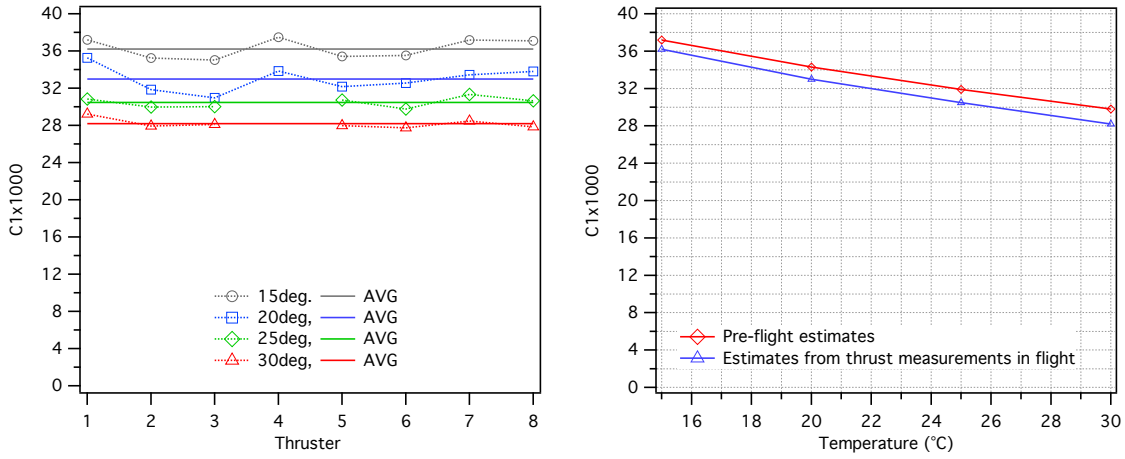


**Figure 11. C1 values estimated from thrust measurements on the spacecraft at different temperatures using "high force" (low resolution) mode.**

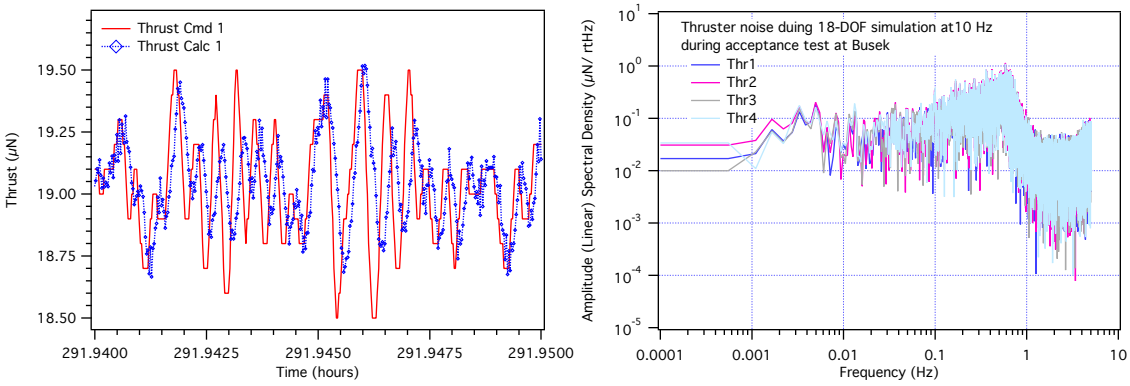


**Figure 12. Thrust command and calculated thrust profiles (left) with thrust noise (right) during ground-based thruster acceptance tests at Busek on Cluster 1, which validate the thruster control algorithm in the control bandwidth (1-30 mHz).**

### B. Thrust Control Algorithm Model Validation Results

The thrust control algorithm was validated in ground tests on each of the eight thrusters during thruster cluster acceptance testing. The thrust command and calculated thrust data are in Figure 12 for Thruster 1. The thrust was calculated from beam voltage and current telemetry using the thruster performance model. The thruster was commanded with simulated 18DoF mode thrust profiles that were expected in flight for about 30 minutes of the acceptance test. Thruster commands were sent at 10 Hz and thruster telemetry was received at 10 Hz. Figure 12 shows commanded and calculated thrust profiles for thruster 1 in the graph on the left, and the data looked similar for the other thrusters. The graph on the right in Figure 12 shows the power spectral density (PSD) of the thrust noise that was calculated for Thrusters 1,2,3, and 4 in Cluster 1. The thrust noise in this analysis is calculated as the difference between the commanded and delivered thrust. The graph shows that all of the thrusters had very similar thrust noise for a largely varying thrust profile. The requirement of $\leq$0.1 $\mu N/\sqrt{Hz}$ in the 1 to 30 mHz frequency band was met by all thrusters. The noise on a constant "DC" thrust command profile was also demonstrated to be as much as an order of magnitude lower.

The control algorithm was validated in flight in all DRS modes by meeting the DRS performance requirements at the system level. Note that for the DRS, the redundancy in the canted directions of the 8 thrusters does not permit distinguishing individual thruster performance, only at the total system level. A sample data set used to verify meeting requirements in 18DoF on DoY 232 are shown in Figure 7. Figure 13 shows thrust command profiles for two thrusters that are nearly DC (static) command profiles from DoY 254 in Zero-G mode. This figure shows both 1 and 10 Hz telemetry, which was only possible for a few 200 second segments due to telemetry volume limitations. Note that one emitter on Thruster 1 briefly obtains a higher thrust level every ~4 s, depending on the current level, because one of the nine emitters was blipping on and off due to a slight blockage that occurred during commissioning. Ground test data did not show this behavior, and investigation continues into the cause of the higher hydraulic impedance on this one emitter since none of the other 71 emitters showed this behavior in the other 7 thrusters. Although it increased thrust noise for Thruster 1, the DRS still met thrust noise performance requirements at the system level. This thrust noise was observable only at 10 Hz as sampling at 1 Hz often missed the emitter blipping events. At 1 Hz sampling, the noise in the PSD spread artificially to lower frequencies. The difference between the thrust noise at 1 and 10 Hz is shown in Figure 14.

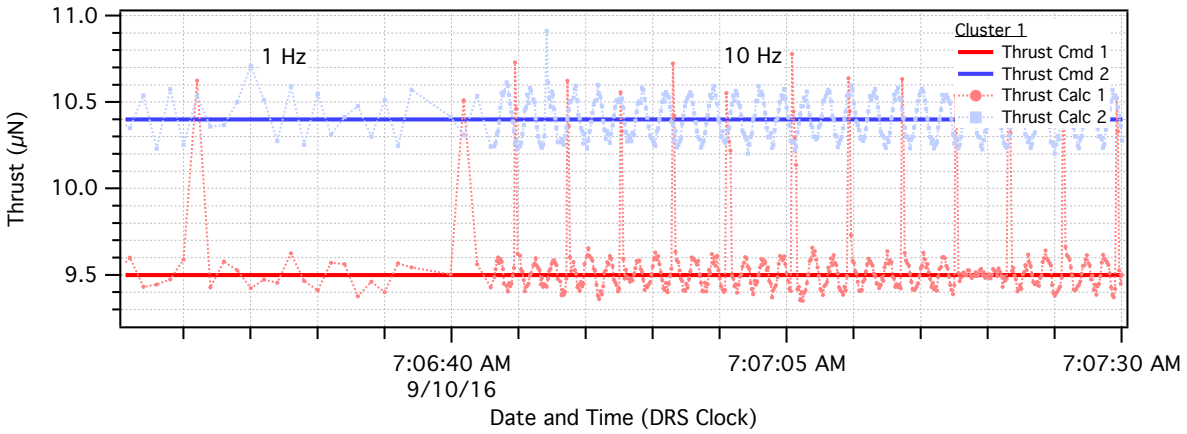


**Figure 13. Command and calculated thrust profiles for thrusters 1 and 2 on DoY 254 (September 10, 2016) in Zero-G mode. The beam voltage is oscillating in the DCIU pass through mode causing most of the noise in data.**

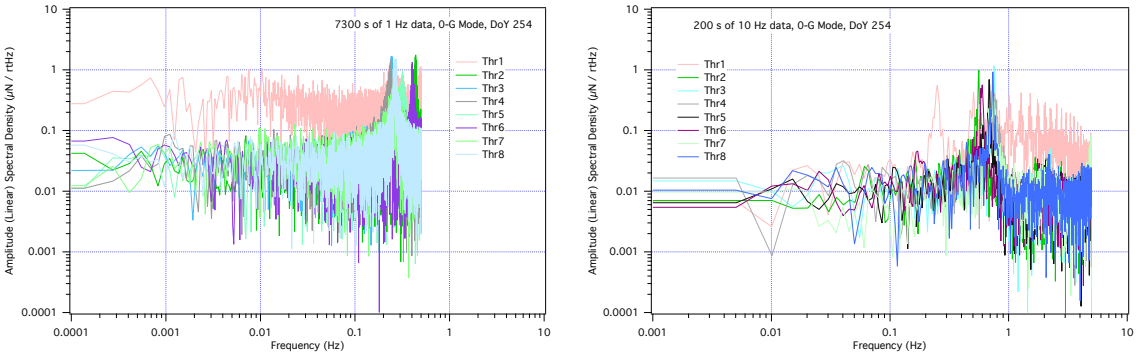


**Figure 14. Thrust noise calculated from 1 and 10 Hz flight telemetry data for all 8 thrusters on DoY 254 2016 (September 10, 2016) in Zero-G mode showing that higher frequency noise (only observable with 10 Hz data) is artificially aliased into the 1 Hz data.**

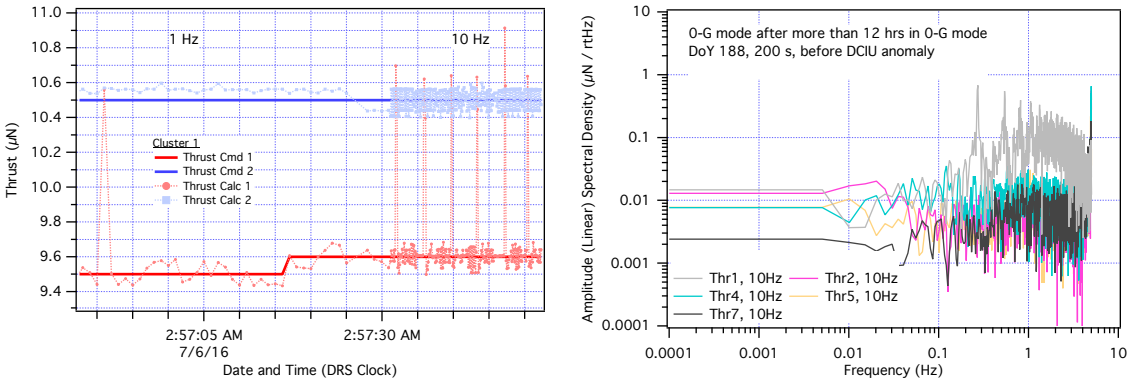


**Figure 15. Command and calculated thrust profiles for thrusters 1 and 2 on DoY 188 (July 6, 2016) in Zero-G mode during instrument commissioning with a fully functional DCIU, before the thruster control algorithm was run on the IAU.**

There is also noise on the calculated thrust for each of the thrusters because of a telemetry delay of ~3 cycles (0.3 s) since the thruster control algorithm was run as part of the flight software in the IAU instead of the DCIU. This delay between the sensing and commanding of the beam voltage, which is designed to adapt to quickly changing thrust commands, led to a predictable triangle-waveform in beam voltage and a slight increase in out-of-band thrust noise. With 10 Hz data, the frequency band of that noise is clearly near ~0.6-0.7 Hz, as shown in Figure 13 and Figure 14. The amplitude is 0.4 μN, or +/- 0.2 μN from the commanded thrust level and clearly out of band for the DCS and requirements. When the telemetry is sampled at only 1 Hz, aliasing causes the frequency of that noise to shift to ~0.3 Hz, which fortunately is still out of the measurement band. Figure 14 shows the thrust noise PSD for that same time over a longer period on DoY 254 in Zero-G mode. The thrust noise PSD is shown for 7300 s of 1 Hz data and 200s of 10 Hz data for comparison. These data verify the noise requirement of 0.1 μN/√Hz in the 1-30 mHz frequency band.

While the noise calculated from the 1 Hz telemetry meets the requirement, the noise estimated from the 200 s of 10 Hz data shows that it is below the requirement at lower frequency. Again, this apparent increase in thrust noise is due to aliasing of the higher-frequency beam voltage noise, which in turn is due to the extra delay in the beam voltage control loop when the IAU is running the thruster control algorithm. Unfortunately, there is only relatively few of the 200 s windows of the 10 Hz data, which makes the PSD on the 10 Hz data unreliable below 20 mHz. Figure 15 shows thrust command and calculated profiles during commissioning, before the DCIU anomaly and telemetry delay. The noise on the calculated thrust has an amplitude of only 0.1 μN instead of 0.4 μN. The PSD of the noise in Figure 15 shows that the thrust noise was significantly lower for all thrusters without the delay, including thruster 1.

The thrust noise was also characterized in 18DoF to validate the control algorithm for that DRS mode where the thrust commands vary quite a bit more due to the finer nature of the control and the feed-forward of noise on the test mass attitude sensing. Thrust noise PSD is shown for 18DoF mode on DoY 115 of 2017 in Figure 16. The thrust noise data in the graph on the left was calculated from 1 Hz telemetry. The data in the graph on the right was calculated from 200 s of 10 Hz data immediately after the 1 Hz data, showing much lower noise without the aliasing issue. These data in the graph on the left in Figure 16 show that all of the thrusters almost met the requirement at 1-30 mHz except for thruster 1; however, the data on the right without the aliasing issue, suggests that they all may have met the requirement. The data in Figure 16 shows that the thrust noise of all of the thrusters is very similar, except Thruster 1.

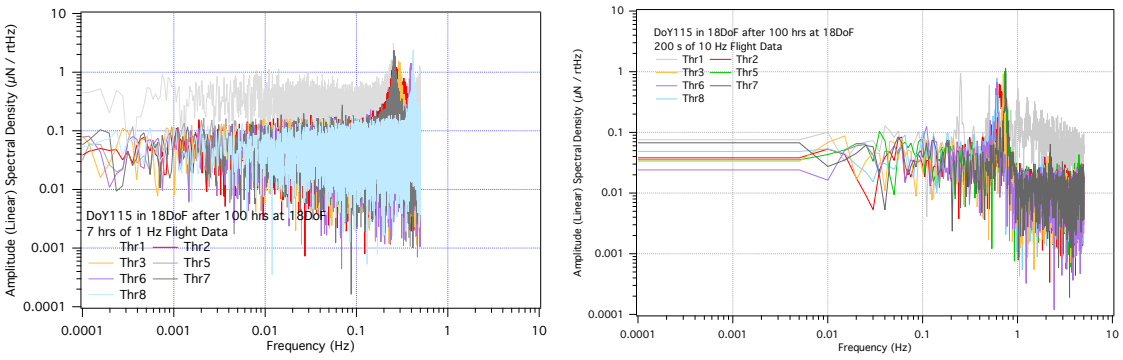


**Figure 16. Thrust noise calculated from 1 and 10 Hz flight telemetry data on DoY 115 (April 25, 2017) in 18DoF Science mode showing the DRS system meeting requirements in the measurement bandwidth (1 – 30 mHz).**

The thruster control algorithm model was verified using both 1 and 10 Hz flight thruster telemetry but showed some differences due to the aliasing issues mentioned previously. In order to understand the performance of the thrusters at lower frequency, but with high rate (10 Hz) data that was not available on orbit, the thruster control algorithm model can be used to simulate thruster response and suggest what the noise spectra could have been in flight at lower frequencies. Figure 17 shows Thruster 5 thrust noise calculated from flight telemetry and from thruster control algorithm simulation results using the same thrust command telemetry from flight. Since the thruster behavior, except for Thruster 1, was so similar, examining one thruster should be representative. In this Figure, thrust noise PSD 1 was calculated from the 1 Hz thrust command and calculated telemetry. Thrust noise PSD 2 was calculated from simulation results using the same thrust command telemetry, but down-sampled at 1 Hz. Note that the simulation runs at 10 Hz, so the 1 Hz thruster command telemetry had to be interpolated to populate a 10 Hz thrust command profile. The noise analysis was done on a 1 Hz sampling of the difference between the calculated and commanded thrust to create the thrust noise PSD 2. The agreement between PSD 1 and 2 provides model validation and shows that the higher frequency noise from the beam voltage triangle waveform bleeds down into lower frequency when down-sampled from 10 to 1 Hz due to aliasing. The thrust noise PSD 3 was created from the 10 Hz simulation results from the same data to show what it could look like if we had 10 Hz telemetry for the 7 hours instead of only 1 Hz flight data. The thruster noise PSD 4 was generated from 200 s of 10 Hz flight data taken immediately after the 7 hours of 1 Hz data. The noise PSD 5 is the result from the simulation of the same 200 s of 10 Hz flight thrust command telemetry. These two results further validate the simulation at higher frequency and match the PSD 3 result that uses the higher frequency data for the longer period.

As mentioned previously, in Figure 17 the noise PSD 1-5 all include the 3-cycle delay in the thruster control loop that produces the ~1 μN peak at ~0.7 s in the 10 Hz data, which then gets spread out at a higher level for the 1 Hz data sampling. The thruster control model algorithm simulation can also be used to examine what the thrust noise would be without the delay. Thrust noise PSD 6 in Figure 17 is the result of running the simulation on the 7 hours of thrust command telemetry without the 3-cycle delay from the flight anomaly in the DCIU. This result suggests that the CMNT thrust noise could be almost an order of magnitude lower than what was demonstrated in flight if the DCIU would have continued to provide its own closed loop control of the beam voltage. It also suggests what thruster 1 noise could have been without both the blipping emitter and DCIU anomalies. The simulation results suggest that the thruster noise was much lower than originally reported by these authors [17] and could be more than 10X lower than requirements without the anomalies.

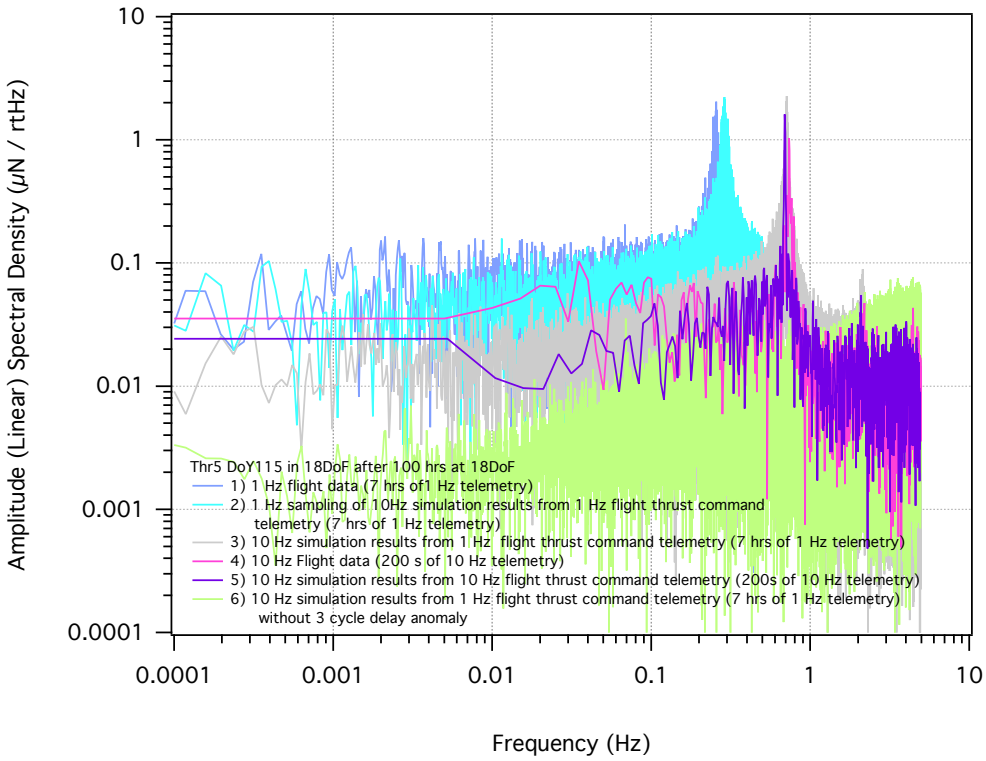


**Figure 17. Thruster 5 noise calculated from flight data (typically at 1 Hz sampling) and from the thruster control model algorithm simulation results sampled at 10 Hz.**

## VI. Conclusion

The ST7-DRS mission demonstrated the CMNT technology and drag free spacecraft control on the LISA Pathfinder spacecraft, including validation of the thruster technology, performance model and control algorithm in flight for the first time. The DRS met the drag-free performance requirement for the mission in providing the LPF spacecraft attitude and drag-free control within position, attitude and thrust requirements. The thrust noise requirement of ≤0.1 μN/√Hz between 1-30 mHz was also verified by direct measurement of test mass motion at the system level and through modeling at the individual thruster level. The performance of all eight CMNTs in flight were consistent with performance during acceptance testing on the ground, except Thruster 1. Thruster 1 had one of nine emitters blipping on and off. Thruster 1 also had a slower response time, both of which are currently under investigation. Individual thruster performance was measured in several experiments over eight months using the gravitational reference sensor on the LPF. The results suggest that the thruster coefficient, $C_1$, is slightly lower than measurements on the ground suggested by approximately 5-10%, which is within the possible error of the GRS force calibration or slightly lower temperature operation in the ground-based tests. The variation in $C_1$ among all eight thrusters throughout the mission was <5% at 25°C. The relative changes in $C_1$ with temperature agreed with pre-flight estimates to within 1.5%. These variations in $C_1$ still proved to be acceptable in the mission because of the closed loop spacecraft control, and because the thrusters met thrust precision and thrust noise requirements.

The thruster control algorithm was also validated in flight with the DRS meeting the mission thrust noise requirement at the system level. Meeting this requirement and characterizing thrust

noise is important because the micro-thrusters are considered to contribute the largest component of noise on the GRS for measuring gravitational waves. The thrust noise measured in flight with actual thrust commands was lower than the measurements on the ground with a simulated 18DoF mode. Measurements in flight validate the control algorithm in meeting the noise requirement in the Zero-G mode and in 18DoF mode except for Thruster 1. However, 10 Hz data over several thousand seconds was required for direct validation and those data were not available. Instead, models validated with 10 Hz data showed that calculated thrust at lower frequencies did meet requirements. There were two DRS anomalies that increased thrust noise: Thruster 1 had a single emitter blipping on and off at about 250 mHz, depending on the current level, and a telemetry delay after a DCIU anomaly [17] caused beam voltage oscillations with a frequency of ~650 mHz. These sources of thrust noise contributed only beyond the measurement band of 1-30 mHz, therefore, they did not affect the system performance in band or prevent it from meeting performance requirements.

A model simulation of the thruster control algorithm was validated with flight data and as a tool to predict CMNT thrust noise. The model simulation was developed in a commercial Wavemetrics Igor data analysis tool and was used to predict thrust noise at critical frequencies where flight data was not available. It was validated with 1 Hz and 10 Hz flight thruster telemetry and verified the contributions by the anomalies to show what the thrust noise would have been without them. These results suggest that the CMNT with their existing performance model and control algorithm are capable of thrust noise levels that are more than 10x lower than the noise requirement for LPF. This model simulation can now be used to consider improvements to the controller to reduce noise further as necessary for the LISA mission or others.

## Acknowledgments

The research described in this paper was carried out by the Jet Propulsion Laboratory, California Institute of Technology, Goddard Space Flight Center and Busek Co., Inc. under contract with the National Aeronautics and Space Administration with our partners in this mission at ESA and on the LPF team. ESA support for the ST7-DRS mission elements and experiments was extraordinary. The authors would also like to thank NASA and the many people that worked on ST7-DRS over the years for their support on the mission.

## References

[1] Danzmann, K. et al, "LISA, Laser Interferometer Space Antenna, A Proposal in Response to the ESA Call for L3 Mission Concepts," January 20, 2017. https://www.eLISAscience.org/files/publications/LISA_L3_20170120.pdf

[2] Armano, M. *et al*., "LISA Pathfinder: the Experiment and the Route to LISA," Classical and Quantum Gravity, Vol. 26, No. 9, 2009.
doi: 10.1088/0264-9381/26/9/094001

[3] Armano, M. *et al*., "Sub-Femto-g Free Fall for Space-Based Gravitational Wave Observatories: LISA Pathfinder Results," Phys. Rev. Lett. 116, 231101, 2016.
doi: 10.1103/PhysRevLett.116.231101

[4] Armano, M. *et al*., "Beyond the Required LISA Free-Fall Performance: New LISA Pathfinder Results down to 20 μHz," Phys. Rev. Lett. 120, 061101, 2018.
doi: 10.1103/PhysRevLett.120.061101

[5] ESA LISA Website, http://sci.esa.int/lisa/

[6] Carmain, A. *et al*., "Space Technology 7 Disturbance Reduction System - Precision Control Flight Validation," *2006 IEEE Aerospace Conference*, Big Sky, MT, 2006, pp. 7.
doi: 10.1109/AERO.2006.1655770

[7] Demmons, N. et al., "ST7-DRS Mission Colloid Thruster Development," *44th AIAA/ASME/SAE/ASEE Joint Propulsion Conference & Exhibit*, Hartford, CT, July 2008. AIAA-2008-4823.
doi: 10.2514/6.2008-4823

[8] Hruby, V., *et al*., "ST7-DRS Colloid Thruster System Development and Performance Summary." *44th AIAA/ASME/SAE/ASEE Joint Propulsion Conference & Exhibit*, Hartford, CT, July 2008. AIAA-2008-4824. doi: 10.2514/6.2008-4824

[9] Ziemer, J. K. *et al*., "Colloid Micro-Newton Thrusters for the Space Technology 7 Mission," *2010 IEEE Aerospace Conference*, Big Sky, MT, 2010, pp. 1-19. doi: 10.1109/AERO.2010.5446760

[10] Hsu, O. C., et. al., "Mode Transitions for the ST7 Disturbance Reduction System Experiment," *AIAA Guidance, Navigation & Control Conference*, Providence, Rhode Island, USA, August 2004. AIAA 2004-5429. doi: 10.2514/6.2004-5429

[11] O'Donnell, J. R., et. al., "The Space Technology 7 Disturbance Reduction System—Precision Control Flight Validation," *Proceedings of the 19th International Symposium on Space Flight Dynamics*, Kanazawa, Japan, June 2006.

[12] Maghami, P.G., et. al., "Drag-Free Control Design for the ST7 Disturbance Reduction System Flight Experiment," *AIAA Guidance, Navigation, and Controls Conf.,* Hilton Head, SC, August 2007. AIAA 2007-6733. doi: 10.2514/6.2007-6733

[13] Demmons, N. R., Lamarre, N., Ziemer, J. K., Parker, M., and Spence, D., "Electrospray Thruster Propellant Feedsystem for a Gravity Wave Observatory Mission," *52nd AIAA/SAE/ASEE Joint Propulsion Conference,* July 25-27, 2016, Salt Lake City, UT, pp. 4739. doi: 10.2514/6.2016-4739

[14] Hsu, O. H., Maghami, P. G., O'Donnell, Jr., J. R., Ziemer, J. K., and Romero-Wolf, A., "Dynamic Control System Performance during Commissioning of the Space Technology 7 - Disturbance Reduction System Experiment of LISA Pathfinder," *40th Annual Guidance and Control Conference*, 3-8 Feb. 2017; Breckenridge, CO.

[15] Maghami, P. G., O'Donnell, Jr., J. R., Hsu, O. H., Ziemer, J. K., and Dunn, C. E., "Drag-Free Performance of the ST7 Disturbance Reduction System Flight Experiment on the LISA Pathfinder," *10th International ESA Conference on Guidance, Navigation & Control Systems*; 29 May - 2 June 2017; Salzburg; Austria.

[16] O'Donnell, Jr., J. R., Hsu, O. H., and Maghami, P. G.,, "Dynamic Control System Mode Performance of the Space Technology 7 Disturbance Reduction System," *68th International Astronautical Congress*, 25–29 September 2017, Adelaide, Australia.

[17] Ziemer, J. K., Marrese-Reading, C., Dunn, C., Romero-Wolf, A., Cutler, C., Javidnia, S., Le, T., Li, I., Franklin, G., Barela, P. and Hsu, O., "Colloid Microthruster Flight Performance Results from Space Technology 7 Disturbance Reduction System," *International Electric Propulsion Conference 2017*, 8-12 Oct. 2017; Atlanta, GA. IEPC 578-2017.

[18] Hruby, V., Demmons, N. R., Courtney, D., Ziemer, J. K., Dunn, C., and Marrese-Reading, C., "Colloid Micronewton Thrusters (CMNTs) – Comparison Between LISA Pathfinder In-Flight and Ground Measurements," *Space Propulsion Conference,* May 14-18, 2018, Seville, Spain. SP2018-00567**.**

[19] Demmons, N. R., Alvarez, N., Courtney, D., Model, J., Hruby, V., and Ziemer, J. K., "Colloid MicroNewton Thruster (CMNT) System Design Updates Towards Meeting LISA Mission Requirements," The 4S Symposium, May 28 – June 1, 2018, Sorrento, Italy.

[20] Marie, J., Cordero, F., Tatry, P., Ecale, E., and Milligan, D. J., "In-orbit Experience of the Gaia and LISA Pathfinder Cold Gas Micro-Propulsion Systems," *2018 SpaceOps Conference*, Marsielle, France, 2018, pp. 2716. doi: 10.2514/6.2018-2716